Journal of Drug Delivery Science and Technology 61 (2021) 102189

Contents lists available at ScienceDirect

Journal of Drug Delivery Science and Technology

journal homepage: www.elsevier.com/locate/jddst

Research paper

Mesoporous zirconia nanoparticles as drug delivery systems: Drug loading, stability and release

Benedetta Leonetti [a,b,**], Alessandro Perin [c], Emmanuele Kizito Ambrosi [a,b], Gabriele Sponchia [a,b], Paolo Sgarbossa [d], Andrea Castellin [a], Pietro Riello [b,c], Alessandro Scarso [c,*]

[a] BRENTA S.r.l. Viale Milano 26, 36075, Montecchio Maggiore, Vicenza, Italy
[b] ECLT Lab - European Centre for Living Technology, University Ca' Foscari of Venice, Via Torino 155/b, 30172, Venice, Mestre, Italy
[c] Dipartimento di Scienze Molecolari e Nanosistemi, Università Ca' Foscari Venezia, Via Torino 155, 30172, Mestre, Venezia
[d] Dipartimento di Ingegneria Industriale, Università Degli Studi di Padova, Via Marzolo 9, 35131, Padova

ARTICLE INFO

Keywords:
Zirconia nanoparticles
Drug delivery systems
Mesoporous material
Drug stability
Drug loading

ABSTRACT

Drug delivery systems have been a milestone in medical research in the last twenty years, still representing a key aspect of innovation and evolution in pharmacokinetics and pharmacodynamics. Among several proposed solutions, inorganic mesoporous materials could be a promising vehicle. Their specific chemical-physical properties make them ideal candidates for the adsorption and loading of active pharmaceutical ingredients (API). Recently, mesoporous zirconia nanoparticles (MZNs) have been described as a novel drug delivery system due to their high surface area and biocompatibility. In this work, we investigated the loading and release efficiencies of a wide range of API on MZNs characterized by suitable pore volume and versatility, focusing on the integrity of the released drugs investigated through solution NMR and ESI-MS techniques. In order to explore the potentialities of MZNs for biomedical applications, we selected ibuprofen, N-acetyl-L-cysteine, vancomycin, gentamicin, nitrofurantoin, and indomethacin as benchmark API characterized by a wide range of polarity, molecular weight and presence of different functional groups. MZNs showed to efficiently load and release most of the API investigated. Long time loadings were also investigated observing that, after more than three months, no side reaction occurred on the released drugs except for intrinsically more labile API like NTF and NAC. MZNs ensured high inertness towards a wide range of functional groups such as aliphatic and aromatic amides, acetals of sugar residues as well as several chiral moieties bearing tertiary stereocenters.

1. Introduction

The most common methods to administer drugs include swallowing and injecting. Between them, traditional drugs available now for oral administrations are not always the optimal formulation. For example, lipophilic oral administered drugs are often considered a challenging task in terms of achieving systemic absorption. In particular, these drugs belong to Biopharmaceutical Classification System (BCS) II, having limited dissolution rate [1]. For pharmaceutical companies, carriers to deliver these API can be a possible solution to overcome the problem of their consequent low bioavailability [2]. These opened the way to drug delivery systems (DDS) and nanotechnologies, whose high surface area and the plethora of possible surface modifications can adsorb and control release conditions for molecules of interest [2,3]. Recent studies are focused on the employment of nanoparticles as DDS and underlined the main advantages of mesoporous carriers based on their structural

Abbreviations: API, active pharmaceutical ingredients; CD_3OD, deuterated methanol; D_2O, deuterated water; DDS, drug delivery systems; DLS, dynamic light scattering; DMF, dimethylformamide; EtOH, ethanol; ESI-MS, electrospray ionization mass spectroscopy; GNTM, gentamicin; HDA, hexadecylamine; IBU, ibuprofen; INDM, indomethacin; M.W, molecular weight; MZNs, mesoporous zirconia nanoparticles; NAC, N-acetyl-L-cysteine; NMR, nuclear magnetic resonance; NTF, nitrofurantoin; NPs, nanoparticles; SEM, scanning electron microscopy; TEM, transmission electron microscopy; VCN, vancomycin; XRPD, X-ray powder diffraction; ZB, zirconium butoxide; ZP, zeta potential.

* Corresponding author. Dipartimento di Scienze Molecolari e Nanosistemi, Università Ca' Foscari Venezia, Via Torino 155, 30172, Mestre, Venezia.
** Corresponding author. BRENTA s.r.l. viale Milano 26, 36075, Montecchio Maggiore, Vicenza, Italy.
E-mail addresses: bele@brenta.net (B. Leonetti), alesca@unive.it (A. Scarso).

https://doi.org/10.1016/j.jddst.2020.102189
Received 13 February 2020; Received in revised form 16 October 2020; Accepted 27 October 2020
Available online 29 October 2020

parameters, such as size, surface area, pore volume and pore distribution. As long as silica nanoparticles are concerned, typical properties are the surface area that often exceed 1000 m^2/g and pore volume in the range 0.5–1.0 cm^3/g [4–12]. These specific features are fundamental to host molecules of different size, shape and steric hindrance. Other physical-chemical properties, such as surface charge or the presence of specific functional groups, can be properly modified to specifically load molecules with peculiar features. The possibility to functionalize with organic moieties both the inner and outer surface of the nanoparticles (NPs) makes them extremely versatile materials for further investigations [7]. For example, surfaces can be made hydrophobic or hydrophilic, or the presence of organic residues could increase the affinity for a specific molecular target or influence the bioavailability or the biodistribution of the NPs. Moreover, different functionalizations could coexist on the same surface, broadening the field of the possible applications [8,9]. In particular, well-known titanium oxide or silicon dioxide NPs could enable sustained and controlled release of the drugs at the site of interest while preserving the stability of the loaded molecules and enhancing their bio-availability for a prolonged time [10–12]. Further advantages could be an improved solubility and biological membrane permeability, a better temporal stability and enhanced therapeutic performance of the drugs, protecting them from degradation. For some specific applications, bio-inert mesoporous carriers could therefore be an interesting choice [1].

While mesoporous silica NPs as DDS has been a highly investigated field of research thanks to the ease of modification of the properties of these NPs, recently introduced Mesoporous Zirconia Nanoparticles (MZNs) have received much lower attention [13–16,17a,b,18–20]. Zirconia is a well-known non-toxic biocompatible material exploited for its properties as bulk, in particular in orthopedics and dentistry, just to name two of the most relevant applications [21–32]. Regarding zirconia NPs, toxicological profile is first of all strongly dependent from their dimensions. For instance, two recent publications investigated ZrO_2 NPs of <100 nm diameter observing toxicity on PC12 and N2a Cells and embryonic development of zebrafish, at concentrations of >31 μg/ml [33] and 0,5–1 μg/ml[34], respectively. Similar results were observed by other authors [35,36]. On the other hand, Yang et al. described intravenous administration of hollow ZrO_2 nanoparticles whose diameter higher than 150 nm without observing toxicity up to 500 mg/kg in mice [37]. MZNs could show important advantages for *in vivo* biomedical applications and for drug loading processes [16]. Recently our group reported about the controlled synthesis of new MZNs and demonstrated their biocompatibility and cell permeability and degradability, making them an ideal candidate for theranostic applications [17a,b]. Based on these results, to assess the real potentialities of MZNs as drug carrier, in the present contribution we report about our investigation on both the loading and the release properties as function of the medium and the molecular structure of the API investigated. In particular, a wide range of Active Pharmaceutical Ingredients (API) was considered characterized by a wide range of polarity, molecular weight, and presence of functional groups (ibuprofen, N-acetyl-L-cysteine, vancomycin, gentamycin, nitrofurantoin, and indomethacin; see Chart 1). Moreover, in consideration of the known acidic and hydrolytic activity of zirconia in aqueous media, we analysed by ESI-MS spectroscopy the integrity of the released API and their stability over time once loaded on the MZNs.

2. Experimental section

2.1. Materials

All reagents were ACS grade and were used as received. Deuterium oxide, methanol-d, dimethylformamide (DMF), acetone, ibuprofen (IBU), zirconium butoxide (ZB), 3-(Cyclohexylamino)-1-propanesulfonic acid (CAPS), sodium acetate, 4-(2-Hydroxyethyl)piperazine-1-ethanesulfonic acid (HEPES), phosphoric acid and acetonitrile HPLC grade were purchased from Sigma-Aldrich. N-acetyl Cysteine (NAC) was purchased from ABCR. Absolute ethanol (EtOH) was purchased from AnalaR Normapur; NaF, and NaCl from Fluka. 1-hexadecylamine (HDA) was purchased from Alfa Aesar. Gentamicin (GNTM) sulfate (40 mg/mL) of Fisiopharma and vancomycin (VCN) of Vancotex (500 mg) were kindly provided by Istituto Ortopedico Rizzoli of Bologna; FIS SpA provided nitrofurantoin (NTF) and indomethacin (INDM). For all aqueous solutions MilliQ water was used.

2.2. Synthesis and characterization of MZNs

The protocol used for the synthesis of MZNs was adapted from the literature [17a,b]. The molar ratio of the reagents ZB: EtOH: H_2O: NaF: HDA was 1 : 750: 20 : 0.02: 2. HDA, used as surfactant, was dissolved in ethanol followed by NaF 0.1 M and MilliQ water, under stirring at room temperature. The precursor zirconium butoxide dissolved in ethanol was added dropwise into the first solution under stirring, observing the mixture turning white due to the formation of the insoluble MZNs. Subsequently, three EtOH washing cycles were performed recovering the particulate by centrifugation (15 min at 12000 rcf). The dried powder, suspended in MilliQ water and ethanol, was heated at 170 °C for 20 h in a Teflon bomb. The collected sample was eventually subjected to a heat vacuum extraction process to remove the residual surfactant HDA. MZNs were extensively characterized by means of field emission-scanning electron microscopy (FE-SEM), transmission electron microscopy (TEM), dynamic light scattering (DLS), Zeta potential (ZP), physisorption of N_2 (BET and BJH) and X-ray powder diffraction (XRPD) analyses.

2.3. Characterization

Size, morphology and sample composition were assessed using a FEG-SEM (Field Emission Gun - Scanning Electron Microscope), Σigma from Zeiss. Mean NPs diameter was calculated measuring at least 500 nanoparticles, using the image analysis software ImageJ. TEM micrographs were collected by JEM 3010 (JEOL) electron microscope at 300 kV of accelerating voltage. The nitrogen adsorption-desorption isotherms were measured at liquid nitrogen temperature, −196 °C, using a Micrometric ASAP 2010 volumetric adsorption analyzer. The specific surface area was calculated from BET equation and the pore size distributions from BJH. DLS and ZP measures were conducted at the University of Verona using Zetasizernano SZ3600 equipped with a laser operating at 633 nm. UV–Vis measurements for drug loading and release measurements were recorded on UV–Vis spectrophotometer Agilent 8453 and Nanophotometer Implen at 280 nm for VNC and 265 nm for IBU. The drug loading efficiencies of NTF, NAC and INDO were calculated by HPLC of PerkinElmer NCI900 equipped by UV–Vis Series 200 detector. GNTM loading was analysed by ^1H NMR due to the lack of suitable chromophores on the API for the UV spectroscopy. All loading efficiencies were also confirmed by quantitative ^1H NMR on the surnatant solutions. A Philips X'Pert vertical goniometer with Bragg Brentano geometry, connected to a highly stabilized generator was used for XRPD measurements. A focusing graphite monochromator and a proportional counter with a pulse-height discriminator were used. Nickel-filtered Cu kα radiation and a step-by-step technique were employed with steps of 0.05° for 10 s from 5 to 140° and steps of 0.02° for 30 s from 32 to 35°.

2.4. Drug loading and release

The drug loading protocol consisted in a simple wet impregnation process obtained through the dispersion of a specific amount of MZNs solution (50 mg/mL) in MilliQ water or in organic solvent containing a known amount of API (starting from a mother solution of 50 mg/mL in MilliQ water for NAC and VCN, ethanol for IBU, acetone for INDM and DMF for NTF). The suspension was stirred for 6 h at room temperature. Afterward, the loaded NPs were separated from the solution by centrifugation (10 min at 12000 rcf). The supernatant was analysed to

calculate the residual concentration of the API thus determining the drug loading as difference. A preliminary study of loading content was carried out by UV–Vis spectroscopy and HPLC and then all the results were confirmed by ^{1}H NMR. UV–Vis spectroscopy was used to detect VCN and IBU loading efficiencies, respectively at 280 and 265 nm. Reverse-phase HPLC methods were used to detect NAC, INDM and NTF using a Nucleosil® 100-5 C18 EC Column thermostatted at 35 °C. Specifically, we used an isocratic elution in phosphoric acid (0.1%)/acetonitrile, with 80:20, 20:80 and 30:70 ratio respectively. Flow rates were respectively 1.0, 1.5 and 1.2 mL/min and ultraviolet detection set at 220, 235 and 254 nm. Finally, the quantitative ^{1}H NMR analyses were used to compare the results of all the drug loading tests. The amount of loaded API was calculated using the following equation:

$$Loading\ content(\%) = \frac{(Initial\ amount\ of\ drug\ (mg) - Residual\ drug\ content\ (mg))}{amount\ of\ MZNs(mg)}\ 100$$

Equation 1 Experimental loading efficiency equation % w/w.

To evaluate the drug release efficiency process, 10 mg of the loaded MZNs were dispersed in 7 mL of D_2O or CD_3OD, according to the solubility of the drugs, in order to have a quantitative release to characterize the molecules. In particular, we need to perform these experiments to investigate if the loading process alter the molecule integrity. The suspension of drug loaded nanoparticles was left under stirring on an oscillating shaker for 24 h at room temperature. At given time intervals, 1 mL of the suspension was withdrawn, centrifuged (10 min at 12000 rcf) and the drug concentration in the supernatant was preliminarily determined by HPLC or UV–Vis spectrophotometer, and then by quantitative ^{1}H NMR. The solution containing the released API was also subjected to ESI-MS analysis to confirm the integrity of the molecules and the presence of possible by-products. The release percentage was calculated by quantitative NMR in solution based on the starting API content, using the following equation:

$$Release(\%) = \frac{amount\ of\ drug\ in\ the\ supernatant\ (mg)}{starting\ drug\ content\ in\ MZNs\ (mg)}100$$

Equation 2 Experimental release efficiency equation % w/w.

In order to identify MZN as possible carrier to administer drugs, we evaluated the long-term stability of released molecules. Specifically, after the loading protocol, the pellets (drug loaded nanoparticles) were collected after centrifugation and stored at 4 °C for 100 days. Then, the loaded particles were suspended in 7 mL of deuterated solvent and the release test was conducted as described before (Equation 2). We compared the integrity of corresponding drugs stored in solution in the same conditions.

2.5. Quantitative ^{1}H NMR analysis and drug stability evaluation by NMR

^{1}H NMR spectra were recorded with a Bruker Ascend 400 spectrometer operating at 400 MHz with saturation of the solvent peak of water at 4.7 ppm. Resonance frequencies are referred to the tetramethylsilane. Quantitative ^{1}H NMR determinations were carried out preparing standard solutions of the API as reported in the drug loading and release section, adding 30% v/v of the proper deuterated solvent (see Table 1). Since the release tests were directly carried out in deuterated solvents, aliquots of 1 mL on the solution obtained at fixed times (0, 30, 60, 120, 240, 420, and 1440 min) were isolated by centrifugation and directly analysed by quantitative NMR with respect to the corresponding loading API reference (mother solutions used of the API in the corresponding deuterated solvent with a concentration in the range 1–5 mM). The comparison allowed immediately to observe that the released API was identical to the reference one. Quantitative determination was carried out using the quantitative Eretic Bruker program acquiring the ^{1}H NMR spectra of the samples and of the references with the same acquisition parameters such as number of scans 16 and d1 of 10 s. For the quantitative analyses in all cases the same resonance for the release drug and the reference were used for the integrations as here detailed: IBU 7.19 ppm (dd), NAC 2.90 ppm (m), GNT 4.17 ppm (dd), NTF 7.16 ppm (d), INDM 7.05 ppm (d), VCN 0.87 ppm (dd).

2.6. ESI MS analyses

ESI MS analyses were performed using a Finnigan LCQ-Duo ion-trap instrument, operating in both positive and negative ion mode (sheath gas flow N_2 30 au, source voltage 4.0 kV, capillary voltage 21 V, capillary temperature 200 °C). The He pressure inside the trap was kept constant. The pressure, directly read by an ion gauge (in the absence of the N_2 stream), was 1.33×10^{-5} torr. Sample solutions were prepared by diluting the supernatant solution with methanol or acetonitrile 1:1 immediately before analysis.

3. Results and discussion

3.1. Synthesis and characterization of MZNs

The synthesis of the MZNs was carried out as recently reported [38]

Table 1
Experimental and theoretical loading efficiencies w/w% for a series of API characterized by different properties. Model 1 provides the maximum theoretical loading efficiency considering the drug density and the total pore volume. Model 2 provides the maximum (A_{Max}) and minimum (A_{Min}) loading % based on the footprint areas of the API considering the formation of a monolayer coverage of the MZNs with a 0.74 coefficient derived by the general packing factor known for close-packed disposal. a) source: Drug bank (www.drugbank.ca).

API	Solvent/buffer	Solubility H_2O (mg/mL)	LogP[a]	Experimental loading efficiency (%)	Model 1 Max. loading (%)	Model 2 Max. loading A_{Max} (%)- A_{Min} (%)
IBU	Ethanol	0.021	3.97	15 ± 5	32	8–15
NAC	MilliQ water	5.09	−0.03	10 ± 3	39	8–13
GNTM	MilliQ water, (acid, basic or neutral buffer)	>50	−3.10	0	32	10–17
NTF	DMF	0.08	−0.47	10 ± 5	49	9–19
INDM	Acetone	0.08	4.27	10 ± 5	37	9–19
VCN	MilliQ water	>50	−3.10	10 ± 2	40	13–20

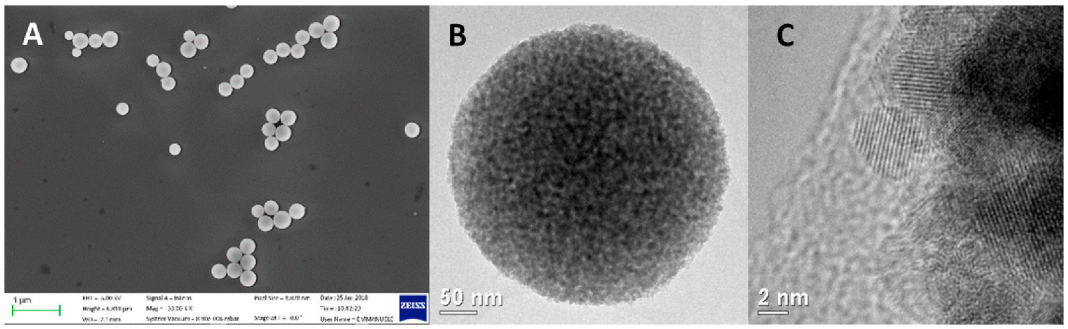

Fig. 1. **A** FE-SEM image of MZNs showing the uniformity in shape and dimension of the sample. **B–C** TEM- HREM analyses of MZNs. In **B** the surface roughness of MZNs is due to its porosity and to the presence of crystallites; **C** detail of the zirconia crystallites.

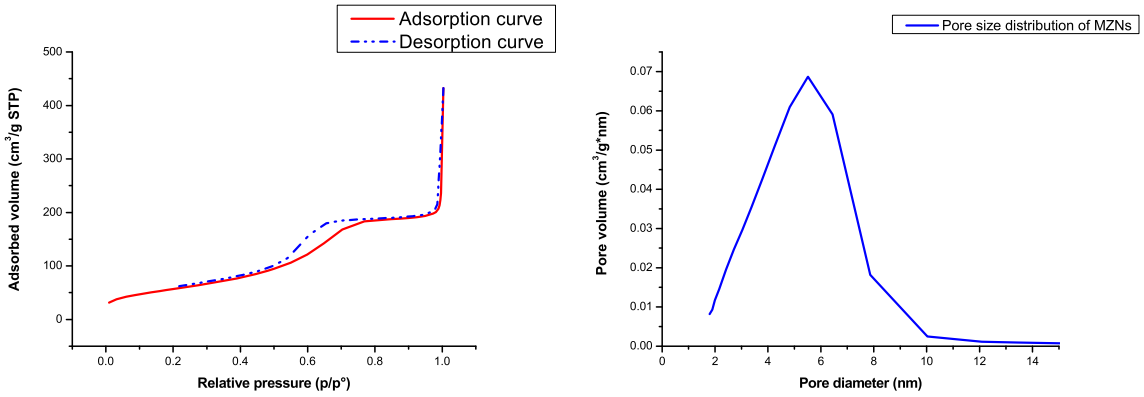

Fig. 2. N_2 physisorption curve of MZNs showing an isotherm of type IV, typical of mesoporous systems (left). The pore size distribution of MZNs determined by adsorption BJH (right).

(see experimental section) and repeated for multiple batches of about 250 mg each. SEM and TEM analyses showed well defined and well-separated porous spherical NPs (Fig. 1). High-resolution TEM analysis showed roughness on MZNs, probably due to their porosity and partial crystallinity as described below. Different synthesis batches gave good reproducibility, with an overall average diameter of 300 ± 70 nm[38].

N_2 adsorption–desorption isotherm of type IV was observed, based on the "Brunauer classification" (or BDDT) with an H1 hysteresis loop, according to the IUPAC classification, typical for mesoporous systems (Fig. 2). The MZNs samples showed an average specific surface area of about 200 ± 20 m^2/g, and an average pore diameter of 5.0 ± 2.0 nm, according to the BJH model applied to the adsorption branch. The pore volume was measured to be 0.31 ± 0.05 cm^3/g.

DLS measurements were carried out in water at neutral pH showing a hydrodynamic diameter for the NPs of 472 ± 20 nm and a polydispersion index (PdI) of 0.46. The larger size observed by DLS with respect to TEM analysis is likely to be due to the presence, as described below, of charges on the surface of the NPs with a consequent larger hydration shell that surrounds the particles and that justify the larger hydrodynamic diameter observed.

The presence of superficial charges on MZNs influences the colloidal stability of the nanoparticles and is also dependent by the pH of the solution. Moreover, surface charge properties of the carrier are important properties to be considered to investigate both the loading and the

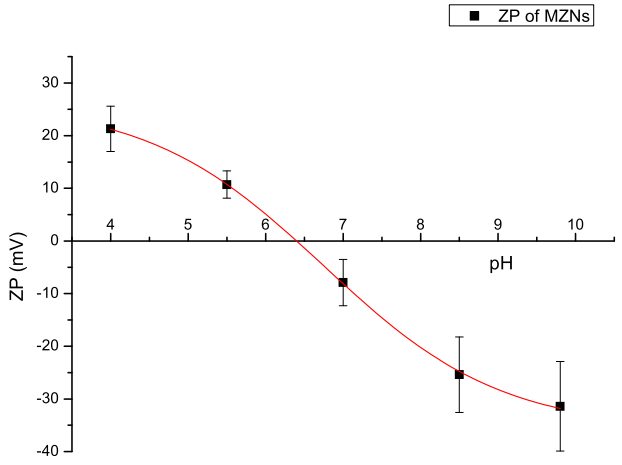

Fig. 3. Zeta Potential of MZNs as a function of pH.

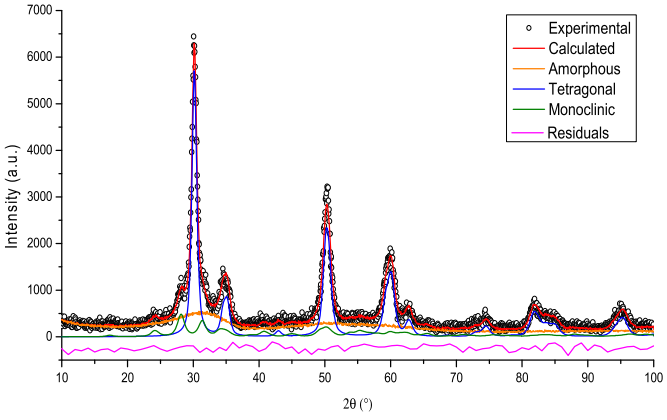

Fig. 4. Rietveld fit of MZNs XRPD analysis. The fit shows the presence of both crystalline (about 30%) and amorphous phases.

release processes of the different APIs. Zeta potential (ZP) measurements is a rapid and straightforward technique to gain information about the electrostatic interactions involving the MZNs. Fig. 3 reports the surface charge of MZNs as a function of the pH of the solution. Under acidic conditions at low pH values, the ZP of the MZNs was positive (25–30 mV). The number of positive superficial charge decreases at higher pH values, with the isoelectric point which falls in the range between pH 6.0 and 7.0. Beyond this point the ZP becomes negatively charged, reaching a plateau of about −30 mV at pH = 10.0.

XRPD analyses were conducted to investigate the crystalline phases of the MZNs. The particles were characterized by the presence of a partial crystalline phase, up to about 30% (Fig. 4). The Rietveld fit showed the presence of both amorphous and crystalline phases, in particular the tetragonal phase with a small amount of monoclinic phase. Usually, in the bulk, the latter phase is more stable than the former, but at the nanoscale level (the crystallite size was about 8 nm) the tetragonal phase could be stabilized as well, without requesting the presence of dopants [39]. The presence of partial crystallinity in the MZNs differs from what previously reported [17a,b]; this could probably be due to the employment of different MZN precursors, specifically different zirconium alkoxides.

3.2. Drug loading

A series of API were selected to represent a large range of therapeutic properties, based on their structural complexity, characterized by a large diversity of functional groups, polarity and solubility in different media. For almost all the API tested, the average size of the pores of the MZNs is more than one order of magnitude larger than the size of the molecules loaded, thus allowing to consider most of the surface and the pore volume of the MZNs accessible by the API. In particular, even the larger API tested, VCN, has an apparent molecular diameter of about 2 nm [40,41], compared to an average pore diameter of about 5 nm.

The loading experiments were carried out as reported in the experimental section, i.e. stirring for 6 h a solution of the drug in the presence of a given amount of MZNs. The loaded NPs were obtained by centrifugation followed by solvent removal. The loading efficiency was calculated by UV–Vis, HPLC and quantitative ^{1}H NMR on the supernatant solution expressed as the ratio between weight of loaded API and weight MZNs (Equation 1). It is worth to notice that in the literature there are examples of extremely high loading efficiencies, obtained simply by drying the solution of the drug with the carrier [42–46]. This method does not imply a true loading process, rather it represents a way to obtain a solid mixture of the drug and the carrier. Differently, in our loading protocols, after each loading, we separated the supernatant solution thus isolating real encapsulated drugs. The results and the loading conditions are reported in Table 1.

Drug loading is influenced by several parameters, such as the solubility and polarity of the API, solvation properties of the solvent and electrostatic interactions with the MZNs for charged drugs. Among other characteristics, the size, shape and surface area of the API as primary properties play a key role in influencing the theoretical maximum loading capacity of the API. To estimate the latter value we used two different models, one related to the total volume of the MZNs accessible by the API (Table 1, model 1), and the other related to the surface area of the MZNs accessible by the API (Table 1, model 2). Specifically, model 1 calculates the maximum theoretical loading capacity as reported in the following equation:

$$\textit{Model 1 Maximum theoretical loading efficiency}\left(\frac{w}{w}\%\right) = \left(\textit{MZN pore volume}\left(\frac{cm^3}{g}\right) * \textit{drug density}\left(\frac{g}{cm^3}\right)\right) 100$$

Model 2 refers to the footprint area (maximum and minimum, see supporting information) calculated using Marvin Sketch software for each API, considering the Van Der Waals radii with respect to the surface area of the carrier as below reported for the case of a hypothetic monolayer surface coverage of the MZNs.

$$\text{N° molecules of API per g of MZNs} = \text{MZN surface area}\left(\frac{m^2}{g}\right) \div \text{API area}\left(m^2\right)$$

$$\text{mol API} = \text{N° molecules} \div \text{Avogadro's Number}$$

$$\textit{Model 2 Maximum Loading efficiency}\left(\frac{w}{w}\%\right) = 0.74 * (\textit{g API per g MZN}) * 100 = \textit{mol API (mol)} * \textit{molecular weight}\left(\frac{g}{mol}\right) * \left(\frac{1}{g}\right) * 100$$

The calculation of the Model 2 maximum loading efficiency takes also into account for a 0.74 coefficient derived by the general packing factor known for close-packed disposal [47]. In Table 1, we summarize all the theoretical loading obtained following these two models as well as the experimental loading efficiencies.

Model 1 treats the MZNs as porous containers that could load drugs by filling the pores with the API forming multi-layer structures with the same packing and density properties of the API in the solid state. It represents the maximum loading capacity, reached only if the whole volume of the pores of MZNs is filled with the drug. The different API show maximum loading efficiency in the range 32–50% w/w. No direct correlation between the maximum loading efficiency % with the molecular size of the API was observed, while higher loading is possible for more packed API in the solid state. Such values are expectedly larger than the measured experimental loading efficiency since Model 1 does not consider, for instance, the pore size distribution or more importantly, the steric interactions between the API with the surface of the carrier and the solvent employed for the loading process. Because of this, a more accurate model is Model 2 based on the minimal and maximal theoretical footprint surface area of the API considering only single layer loading efficiencies of the API tested. The values comprise a range that is not affected very much by the size of the API, with average values in the range 11–17% with smaller values for smaller API and *vice versa* due to the fact that the larger the molecule and the higher weight gain is obtained loading the specific API.

To promote the drug uptake, solvents were chosen essentially based on the corresponding API solubility in order to maximize their concentration in the loading solution. In order to further comparatively analyze

the data, the logP for the different API is also reported in Table 1. The loading efficiency did not follow a trend with the logP values. For example, the two most hydrophilic API like GNTM and VCN show a completely different affinity for the MZNs, while two API like IBU and NTF, with rather different logP values, show similar loading efficiencies. Overall, the logP value alone cannot be considered a reliable parameter to rationalize the loading efficiency. Rather more detailed analyses should be carried out considering *in primis* the presence of charges on the API with respect to the charges on the MZNs and the presence of large hydrophobic surfaces on the API that can interact with the surface of the MZNs.

Analyzing more into detail the experimental loading efficiencies for the series of API, only GNTM in the form of the corresponding sulfate salt did not show any loading. This is probably due to its aminoglycoside structure characterized by a highly hydrophilic bis-cationic nature and the lack of hydrophobic surfaces that forced the molecule to reside in water without showing interactions with the surface of the MZNs. Attempts were made to force the loading using solutions of GNTM at different pH. While at acidic and neutral pH GNTM is positively charged and this hampers its adsorption process on the MZNs, at high pH we expected to maximize the neutral form of the API in solution [48] and to promote the presence of negative charges on the MZNs based on the ZP measurements (Fig. 3), but no loading was observed in any case. All the other API examined showed loading efficiencies in the range 10–15% that is also comparable with the loading efficiencies calculated with Model 2 considering the footprint area of the API. In order to better appreciate the comparison between experimental and theoretical loading, in Fig. 5 are reported both values for the series of API considered. For IBU and NAC there is a good matching between experimental and theoretical loading efficiency. In fact, both molecules are characterized by a polar carboxylic acid unit that is likely to be deprotonated in water at neutral pH and that could directly interact with the superficial zirconium atoms of the MZNs and a less polar portion that would further favor the adsorption process possibly driven by the hydrophobic effect of water. For NTF and INDM the theoretical values are slightly overestimating the loading efficiency with respect to the experimental values. This difference could also be related to the fact that both API are poorly soluble in water and because of this the loading processes were carried out in acetone (with for NTF 20% v/v of DMF), a solvent that efficiently competes for hydrophobic interactions between apolar portions of the drugs and the surface of the MZNs. As long as VCN is concerned, the distribution of the charges on the drug as a function of the pH of the solution shows a parallel trend with that of the MZNs, thus making favorable its loading at neutral pH, where both the API and MZNs are basically neutral. For VCN the first comparison between theoretical and

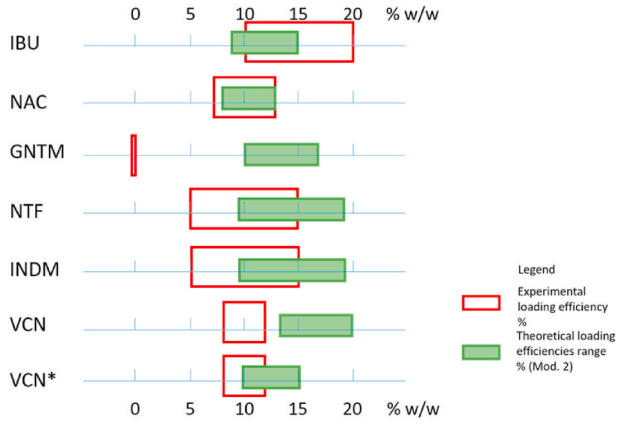

Fig. 5. Experimental (red) vs. theoretical (green) loading efficiency (%) ranges. The VCN*data considering the dimerization of VCN in solution. (For interpretation of the references to colour in this figure legend, the reader is referred to the Web version of this article.)

experimental loading efficiency does not show matching between the two values. This could be ascribable to the very large size of the API, in particular if considering the solvated molecule in water which is larger than 2 nm, thus being excluded by a fraction of the pores of the MZNs (see Fig. 2). It can be estimated that about 10% of the pore volume will be not accessible to VCN. Moreover, at the concentrations used for the loading process, VCN could also form dimers in solution [49], further decreasing the range of accessible pores up to 25% of the available pore volume. Considering the latter observations, these will lower the theoretical maximum loading efficiency to 10–15%, which is a range that fits with the experimental loading efficiency (Fig. 5: VCN*). The above considerations suggest that in general solvation effects as well as spontaneous aggregation phenomena of the API in solution need to be considered for reliable estimation of loading efficiency, especially for API characterized by high molecular weight.

3.3. API release efficiency and stability

The release process was carried out dispersing 10 mg of loaded MZNs in 7 mL of deuterated water for API that were loaded in the same solvent, in some cases controlling the pH of the aqueous solution, or in deuterated methanol, according to drug solubility. The suspensions were stirred, and samples of 1 mL were taken at fixed time, centrifuged to isolate the supernatant solution for direct quantitative NMR determination of the API content. Table 2 reports the release conditions and % w/w of release efficiencies calculated using Equation 2. The release process was monitored after determined time intervals and we observed for all APIs a plateau profile after 2–4 h with unaltered released drug after 24 h, thus we decided to report the release efficiency in Table 2. In Supporting Information, we reported the release profile of all APIs (see Fig. S2), conducted in different experimental conditions in order to simulate API behaviour in physiological conditions.

IBU turned out to be only partially released in D_2O from the MZNs, thus confirming its high affinity for the carrier as a combination of the possible coordination of the carboxylic moiety on superficial Zr atoms and the presence of a hydrophobic portion that well interacts with the surface of the NPs. To improve the release of the API, the experiment was repeated using deuterated methanol observing a quantitative release within 4 h. Since IBU does not contain any labile functional group that could be hydrolyzed, the released IBU turned out to be completely unaffected by the MZNs, as further evidenced by the ^{1}H NMR spectra (see supporting information).

NAC is very soluble in water and it showed almost 80% release after 30 min and quantitative release after 4 h in D_2O. NAC is a rather stable API, nevertheless in solution it is susceptible of thiol oxidation in the presence of air providing the corresponding disulfide acetylated cystine derivative. ^{1}H NMR spectra showed that the released species did not show detectable traces of the cystine derivative (see supporting information). This confirms the stability of the acetamido moiety present in NAC as well as the thiol moiety once loaded on the MZNs.

Being NTF scarcely soluble in water, the release experiments were carried out in deuterated methanol observing a quantitative release within 4 h. Due to the presence of an imine moiety, this API is intrinsically less stable and susceptible of hydrolysis [50–52]. The ^{1}H NMR spectra (see supporting information) showed no alteration for the released API for up to 4 h, while for longer release tests some degradation of the molecule (up to 14%) was observed as evidenced by the presence of new resonances at 7.22 ppm and others overlapped at 7.56 ppm. The degradation is therefore not related to the loading process since at the beginning of the release test, after 30 min, the ^{1}H NMR spectrum of the API in solution perfectly matched that of the original NTF. It is likely that partial decomposition of NTF takes place once the API is in solution for several hours. ESI-MS analysis did not provide a clear-cut description of the side products observed due to scarce solubility in the solvent and poor ionization in acetone. Nevertheless, more accurate observation of the ^{1}H NMR new resonances suggested the

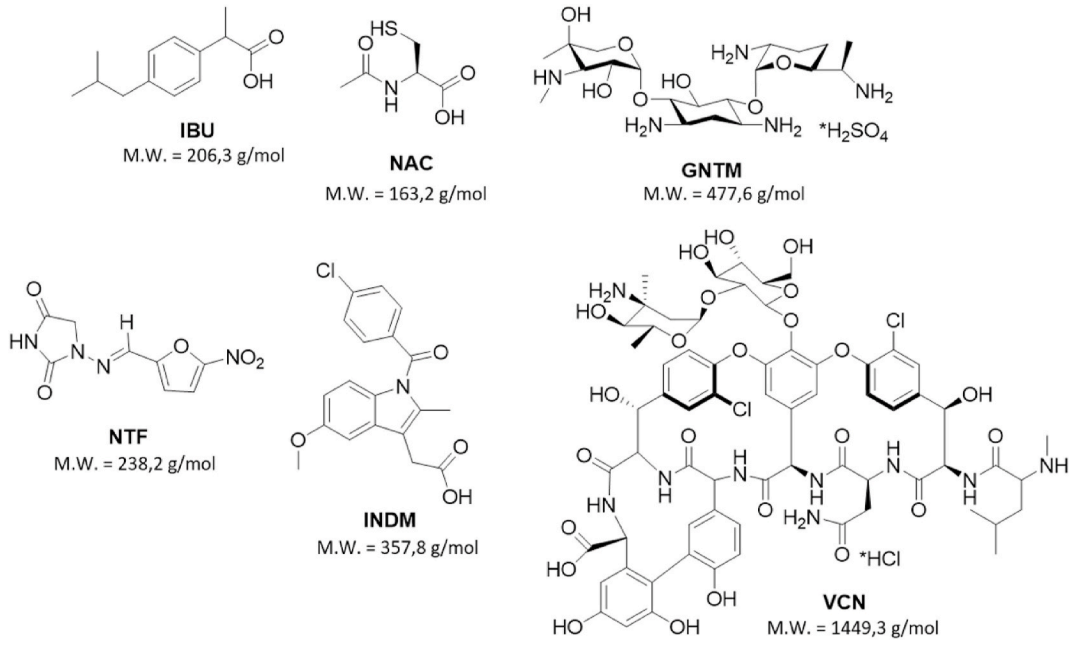

Chart 1. molecular structures of the API investigated.

formation of the hydrolysis products due to imine cleavage forming the corresponding furyl-aldehyde and the heterocyclic amine.

For INDM the release was monitored in deuterated methanol due to its low solubility in water [53], observing a 44% release after 4 h with no significant degradation of the API (see supporting information). It is known in the literature that INDM is sensitive to decarboxylation under heating or UV irradiation, which is a common reaction for β,γ-unsaturated carboxylic acids compounds [54]. Moreover, no cleavage of the aromatic amide bond was observed, thus further confirming the stability of this kind of functional group when loaded in the MZNs, as similarly observed for the amide bond of NAC.

VCN is a complex API with a large molecular weight comprising several functional groups like several amide bonds as well as two sugar residues. The release experiments in deuterated water showed quantitative release in 4 h. From the ^{1}H NMR release tests it is clear that VCN is basically unaffected by the loading process. Both the aromatic region of the spectrum and the resonances attributed to the aliphatic alkyl chains of the amino acids of the drug are identical to those of the original API. This confirms that the drug does not undergo any hydrolytic decomposition once loaded on the MZNs.

Overall, the release process of the loaded API showed to be efficient with quantitative release for NAC, VCN in deuterated water and for IBU and NTF in deuterated methanol. Another crucial observation is the high inertness of the MZNs towards a wide range of functional groups such as aliphatic and aromatic amides, acetals of sugar residues as well as several chiral moieties bearing tertiary stereocenters. Only an intrinsically weak API like NTF, known to be subjected to hydrolysis on the imide bond even in pure water, showed minor decomposition.

Table 2
Release efficiency for a series of API loaded on MZNs characterized by different polarity, solubility and variety of functional groups. a) after 4 h; b) NMR integration of the resonances of the fragments with respect to the original API.

API	Solvent	API release efficiency (w/w %)[a]	Integrity of released drug (%)[b]
IBU	D_2O	6	100
IBU	CD_3OD	100	100
NAC	D_2O	100	100
NTF	CD_3OD	100	86
INDM	CD_3OD	44	100
VCN	D_2O	100	100

3.4. Long-term stability of the loaded API in the MZNs

A fundamental property of a pharmaceutical product is its shelf-life [55] that is the period of time that its physical-chemical properties remain unaffected or within certain specifications after manufactures. Considering MZNs as a potentially new carrier to administer drugs, we investigate the stability of the loaded API once released by the NPs after storing at 4 °C for 100 days the pellets.

The results are reported in Table 3.

The stability of the API loaded on the MZNs is directly connected to the stability and robustness of the chemical structures. While for IBU and VCN no differences were observed for the stock solution and the released API after more than three months, indicating that for the period of time considered no side reaction occurred on the drugs loaded on the MZNs, for intrinsically more labile API like NTF and NAC new species were detected both for the stock solution and for the released API, with a slightly larger amount of side products in the latter samples compared to the stock solutions (Table 3). Some ESI-MS analyses were carried out in particular for the released API that confirmed the presence of the side products in solution. Specifically, for NTF, whose higher lability is known (see Table 2), we observed the formation of new aromatic species (about 20% of the total API) arising from the nitro-furane ring both for

Table 3
Integrity % of drugs released from MZNs after 24 h (after storing at 4 °C for 100 days). The integrity was evaluated taking as reference the control such as the 100% stability. a) NMR integration of the resonances of the fragments with respect to the original API, b) the new species detected in solution is the corresponding disulfide derivative of NAC; c) two new nitro-furane derivatives were detected as side products.

API	Solvent	Integrity of the API stock solutions after 100 days (%)[a]	Integrity of the released API after 100 days (%)[a]
IBU	CD_3OD; D_2O	100	100
NAC	D_2O	83[b]	66[b]
NTF	CD_3OD	77	70[c]
INDM	CD_3OD	100	>98
VCN	D_2O	100	100

the stored mother solution as well as for the released API from MZNs after 100 days. Moreover, in the released sample two sets of new nitrofurane was observed, probably arising from the possible hydrolysis of the imine bond of the API leading to the corresponding aldehyde which could be susceptible of oxidation forming the corresponding carboxylic acid. The fact that no traces for the 1-aminoimidazolidine-2,4-dione heterocyclic ring in solution were observed as counterpart of the possible hydrolysis could be due to its possibly strong affinity for MZNs that prevent its release in solution. For NAC it is known that in solution the API tend to form the corresponding disulfide compound, and this was largely detected in the released NAC after 100 days. As long as INDM is concerned, after 100 days the released API showed mostly retention of the original structure with only traces of a minor aromatic side products (<2%) that could arise by a photodegradation that is possible for this API [54].

4. Conclusions

In conclusion, we described the potentialities of MZNs as a drug carrier for a wide series of API, investigating in detail the loading capacity on the basis of different loading models, the release efficiency as a function of the structural properties of the API investigated, characterized by a wide variability of polarity, solubility and functional group. The integrity of the released drug from the DDS is fundamental for its application and local administration, to exploit its therapeutic properties in the site of interest. Loaded API showed a quantitative release for NAC, VCN in deuterated water and for IBU and NTF in deuterated methanol. We also studied the integrity of the molecules after three months from their loading, comparing it with equally stored samples. For the period of time considered no side reaction occurred on the drugs loaded on the MZNs except for more labile API like NTF and NAC.

Overall, we observed that for efficient loading on MZNs the key features of the drug should be a sufficient solubility in water but also the presence of apolar portions of the molecule that could favor hydrophobic interaction with the surface. Moreover, attention need to be paid to the presence of charges on the API and the matching with the charge properties of the MZNs at different pH values. A further important aspect for the loading is the possible presence on the API of coordinating moieties that could favor the interaction with superficial Zr atoms such as carboxylic units. The release process turned out to be complete for most of the API within a few hours. MZNs ensured high inertness towards a wide range of functional groups such as aliphatic and aromatic amides, acetals of sugar residues as well as several chiral moieties bearing tertiary stereocenters.

Declaration of interests

The authors declare that they have no known competing financial interests or personal relationships that could have appeared to influence the work reported in this paper.

CRediT authorship contribution statement

Benedetta Leonetti: Conceptualization, Writing - review & editing, Investigation, Formal analysis. **Alessandro Perin:** Methodology, Data curation, Formal analysis. **Emmanuele Kizito Ambrosi:** Methodology, Data curation. **Gabriele Sponchia:** Methodology, Data curation, Formal analysis. **Paolo Sgarbossa:** Methodology, Data curation, Formal analysis. **Andrea Castellin:** Conceptualization, Funding acquisition. **Pietro Riello:** Conceptualization, Funding acquisition. **Alessandro Scarso:** Conceptualization, Writing - original draft, Writing - review & editing, Investigation, Formal analysis.

Declaration of competing interest

The authors have no conflict of interest to declare.

Acknowledgements

The authors acknowledge Dr. D. Cristofori for TEM analyses and M. Marchiori for BET analyses. Università Ca' Foscari, Ministero dell'Università e della Ricerca and Brenta srl are gratefully acknowledged for support.

Appendix A. Supplementary data

Supplementary data to this article can be found online at https://doi.org/10.1016/j.jddst.2020.102189.

References

[1] S.A. Rizvi, A.M. Saleh, Applications of nanoparticle systems in drug delivery technology, Saudi Pharmaceut. J. 26 (2018) 64–70, https://doi.org/10.1016/j.jsps.2017.10.012.
[2] C.A. McCarthy, R.J. Ahern, R. Dontireddy, K.B. Ryan, A.M. Crean, Mesoporous silica formulation strategies for drug dissolution enhancement: a review, Expet Opin. Drug Deliv. 13 (2016) 93–108, https://doi.org/10.1517/17425247.2016.1100165.
[3] H. Wen, H. Jung, X. Li, Drug delivery approaches in addressing clinical pharmacology-related issues: opportunities and challenges, AAPS J. 17 (2015) 1327–1340, https://doi.org/10.1208/s12248-015-9814-9.
[4] G. Tiwari, R. Tiwari, B. Sriwastawa, L. Bhati, S. Pandey, P. Pandey, S.K. Bannerjee, Drug delivery systems: an updated review, Int. J. Pharm. Investig. 2 (2012) 2, https://doi.org/10.4103/2230-973X.96920.
[5] M. Vallet-Regí, M. Colilla, I. Izquierdo-Barba, M. Manzano, Mesoporous silica nanoparticles for drug delivery: current insights, Molecules 23 (2018) 47, https://doi.org/10.3390/molecules23010047.
[6] H. Jahangirian, E.G. Lemraski, T.J. Webster, R. Rafiee-Moghaddam, Y. Abdollahi, A review of drug delivery systems based on nanotechnology and green chemistry: green nanomedicine, Int. J. Nanomed. 12 (2017) 2957, https://doi.org/10.2147/IJN.S127683.
[7] C. Bharti, U. Nagaich, A.K. Pal, N. Gulati, Mesoporous silica nanoparticles in target drug delivery system: a review, Int. J. Pharm. Investig. 5 (2015) 124, https://doi.org/10.4103/2230-973X.160844.
[8] S. Shen, Y. Wu, Y. Liu, D. Wu, High drug-loading nanomedicines: progress, current status, and prospects, Int. J. Nanomed. 12 (2017) 4085, https://doi.org/10.2147/IJN.S132780.
[9] S. Balasubramanian, B. Gurumurthy, A. Balasubramanian, Biomedical applications of ceramic nanomaterials: a review, Int. J. Pharma Sci. Res. 8 (2017) 4950–4959, https://doi.org/10.13040/IJPSR.0975-8232.8(12).4950-59.
[10] D. Awotwe-Otoo, A.S. Zidan, Z. Rahman, M.J. Habib, Evaluation of anticancer drug-loaded nanoparticles characteristics by non-destructive methodologies, AAPS PharmSciTech 13 (2012) 611–622, https://doi.org/10.1208/s12249-012-9782-7.
[11] O. Kayser, A. Lemke, N. Hernandez-Trejo, The impact of nanobiotechnology on the development of new drug delivery systems, Curr. Pharmaceut. Biotechnol. 6 (2005) 3–5, https://doi.org/10.2174/1389201053167158.
[12] Y. Li, H. Zhang, Nanoparticle-based drug delivery systems for enhanced tumor-targeting treatment, J. Biomed. Nanotechnol. 15 (2019) 1–27, https://doi.org/10.1166/jbn.2019.2670.
[13] B. Yang, Y. Chen, J. Shi, Mesoporous silica/organosilica nanoparticles: synthesis, biological effect and biomedical application, Mater. Sci. Eng. R. 137 (2019) 66–105, https://doi.org/10.1016/j.mser.2019.01.001.
[14] G. Sponchia, R. Marin, I. Freris, M. Marchiori, E. Moretti, L. Storaro, P. Canton, A. Lausi, A. Benedetti, P. Riello, Mesoporous silica nanoparticles with tunable pore size for tailored gold nanoparticles, J. Nanoparticle Res. 16 (2014) 2245, https://doi.org/10.1007/s11051-014-2245-1.
[15] I. Manavitehrani, A. Schindeler, M. Parviz, Mesoporous silica nanoparticles: synthesis, modification and applications, Nanomed. Nanotechnol. 3 (2018) 1–10, https://doi.org/10.23880/NNOA-16000136.
[16] T. Li, S. Shi, S. Goel, X. Shen, X. Xie, Z. Chen, H. Zhang, S. Li, X. Qin, H. Yang, C. Wu, Recent advancements in mesoporous silica nanoparticles towards therapeutic applications for cancer, ACTA Biomat 89 (2019) 1–13, https://doi.org/10.1016/j.actbio.2019.02.031.
[17] a) G. Sponchia, E. Ambrosi, F. Rizzolio, M. Hadla, A. Del Tedesco, C.R. Spena, G. Toffoli, P. Riello, A. Benedetti, Biocompatible tailored zirconia mesoporous nanoparticles with high surface area for theranostic applications, J. Mater. Chem. 3 (2015) 7300–7306, https://doi.org/10.1039/c5tb01424g.b)Patent WO2016120795.
[18] K.B. Devi, K. Singh, N. Rajendran, Sol–gel synthesis and characterisation of nanoporous zirconium titanate coated on 316L SS for biomedical applications, J. Sol. Gel Sci. Technol. 59 (2011) 513, https://doi.org/10.1007/s10971-011-2520-x.
[19] S. Jafari, H. Derakhshankhah, L. Alaei, A. Fattahi, B.S. Varnamkhasti, A. A. Saboury, Mesoporous silica nanoparticles for therapeutic/diagnostic applications, Biomed, Pharma 109 (2019) 1100–1111, https://doi.org/10.1016/j.biopha.2018.10.167.
[20] Y. Zhang, J. Wang, X. Bai, T. Jiang, Q. Zhang, S. Wang, Mesoporous silica nanoparticles for increasing the oral bioavailability and permeation of poorly

water soluble drugs, Mol. Pharm. 9 (2012) 505–513, https://doi.org/10.1021/mp200287c.
[21] C.M. Cristache, M. Burlibasa, G. Cristache, S. Drafta, I.A. Popovici, A.A. Iliescu, S. Zisi, L. Burlibasa, Zirconia and its biomedical applications, Met. Int. 16 (2011) 18, https://doi.org/10.1080/17434440.2016.1230017.
[22] P.D.L. Mercera, J.G. Van Ommen, E.B.M. Doesburg, A.J. Burggraaf, J.R.H. Ross, Zirconia as a support for catalysts. Evolution of the texture and structure on calcination in air, Appl. Catal. 57 (1990) 127–148, https://doi.org/10.1016/S0166-9834(00)80728-9.
[23] P.D.L. Mercera, J.G. Van Ommen, E.B.M. Doesburg, A.J. Burggraaf, J.R.H. Ross, Zirconia as a support for catalysts: influence of additives on the thermal stability of the porous texture of monoclinic zirconia, Appl. Catal. 71 (1991) 363–391, https://doi.org/10.1016/0166-9834(91)85092-A.
[24] I. Freris, P. Riello, F. Enrichi, D. Cristofori, A. Benedetti, Synthesis and optical properties of sub-micron sized rare earth-doped zirconia particles, Opt. Mater. 33 (2011) 1745–1752, https://doi.org/10.1016/j.optmat.2011.06.010.
[25] R.A. Comelli, C.R. Vera, J.M. Parera, Influence of ZrO2 crystalline structure and sulfate ion concentration on the catalytic activity of So2−4- ZrO2, J. Catal. 151 (1995) 96–101, https://doi.org/10.1006/jcat.1995.1012.
[26] K. Tomishige, Y. Ikeda, T. Sakaihori, K. Fujimoto, Catalytic properties and structure of zirconia catalysts for direct synthesis of dimethyl carbonate from methanol and carbon dioxide, J. Catal. 192 (2000) 355–362, https://doi.org/10.1006/jcat.2000.2854.
[27] L.E. Davies, N. A Bonini, S. Locatelli, E.E. Gonzo, Characterization and catalytic activity of zirconium dionide prepared by sol-gel, Lat. Am. Appl. Res. 35 (2005) 23–28.
[28] P. Bansal, G.R. Chaudhary, S.K. Mehta, Comparative study of catalytic activity of ZrO2 nanoparticles for sonocatalytic and photocatalytic degradation of cationic and anionic dyes, Chem. Eng. J. 280 (2015) 475–485, https://doi.org/10.1016/j.cej.2015.06.039.
[29] K. Shehzad, M. Ahmad, C. Xie, D. Zhan, W. Wang, Z. Li, W. Xu, J. Liu, Mesoporous zirconia nanostructures (MZN) for adsorption of As(III) and As(V) from aqueous solutions, J. Hazard Mater. 373 (2019) 75–84, https://doi.org/10.1016/j.jhazmat.2019.01.021.
[30] S. Shan, H. Tang, Y. Zhao, W. Wang, F. Cui, Highly porous zirconium-crosslinked graphene oxide/alginate aerogel beads for enhanced phosphate removal, Chem. Eng. J. 359 (2019) 779–789, https://doi.org/10.1016/j.cej.2018.10.033.
[31] S. Priyadarsini, S. Mukherjee, M. Mishra, Nanoparticles used in dentistry: a review, J. Oral Biol. Craniofac. Res. 8 (2018) 58–67, https://doi.org/10.1016/j.jobcr.2017.12.004.
[32] J. Chevalier, What future for zirconia as a biomaterial? Biomaterials 27 (2006) 535–543, https://doi.org/10.1016/j.biomaterials.2005.07.034.
[33] E. Asadpour, H.R. Sadeghnia, A. Ghorbani, M. Sedaghat, M.T. Boroushaki, Oxidative stress-mediated cytotoxicity of zirconia nanoparticles on PC12 and N2a cells, J. Nanoparticle Res. 18 (2016) 14, https://doi.org/10.1007/s11051-017-3971-y.
[34] P. Karthiga, M. Ponnanikajamideen, R.S. Rajendran, G. Annadurai, S. Rajeshkumar, Characterization and toxicology evaluation of zirconium oxide nanoparticles on the embryonic development of zebrafish, Danio rerio, Drug Chem. Toxicol. 42 (2019) 104–111, https://doi.org/10.1080/01480545.2018.1523186.
[35] M. Mishra, D. Sabat, B. Ekka, S. Sahu, P. Unnikannan, P. Dash, Oral intake of zirconia nanoparticle alters neuronal development and behaviour of Drosophila melanogaster, J. Nanoparticle Res. 19 (2017) 282, https://doi.org/10.1007/s11051-017-3971-y.
[36] M. Ye, B. Shi, Zirconia nanoparticles-induced toxic effects in osteoblast-like 3T3-E1 cells, Nanoscale Res. Lett. 13 (2018) 1–12, https://doi.org/10.1186/s11671-018-2747-3.
[37] Y. Yang, H. Bao, Q. Chai, Z. Wang, Z. Sun, C. Fu, Z. Liu, Z. Liu, X. Meng, T. Liu, Toxicity, biodistribution and oxidative damage caused by zirconia nanoparticles after intravenous injection, Int. J. Nanomed. 14 (2019) 5175–5186, https://doi.org/10.2147/IJN.S197565.
[38] A. Del Tedesco, V. Piotto, G. Sponchia, K. Hossain, L. Litti, D. Peddis, A. Scarso, M. Meneghetti, A. Benedetti, P. Riello, Zirconia-based magneto plasmonic nanocomposites: a new nanotool for magnetic guided separations with SERS identification, ACS Appl. Nano Mater. 3 (2020) 1232–1241, https://doi.org/10.1021/acsanm.9b01982.
[39] R.C. Garvie, The occurrence of metastable tetragonal zirconia as a crystallite size effect, J. Phys. Chem. 69 (1965) 1238–1243, https://doi.org/10.1021/j100888a024.
[40] M. Schäfer, T.R. Schneider, G.M. Sheldrick, Crystal structure of vancomycin, Structure 4 (1996) 1509–1515, https://doi.org/10.1016/s0969-2126(96)00156-6.
[41] P.J. Loll, A. Derhovanessian, M.V. Shapovalov, J. Kaplan, L. Yang, P.H. Axelsen, Vancomycin forms ligand-mediated supramolecular complexes, J. Mol. Biol. 385 (2009) 200–211, https://doi.org/10.1016/j.jmb.2008.10.049.
[42] C.A. McCarthy, R.J. Ahern, R. Dontireddy, K.B. Ryan, A.M. Crean, Mesoporous silica formulation strategies for drug dissolution enhancement: a review, Expet Opin. Drug Deliv. 13 (2016) 93–108, https://doi.org/10.1517/17425247.2016.1100165.
[43] S. Shawky, A.A. Abo-alHassan, H. Lill, D. Bald, S.F. El-Khamisy, E.Z.M. Ebeid, Efficient loading and encapsulation of anti-tuberculosis drugs using multifunctional mesoporous silicate nanoparticles, Int. J. Nanosci. 1 (2016) 1, https://doi.org/10.4172/jncr.1000103.
[44] T. Limnell, H.A. Santos, E. Mäkilä, T. Heikkilä, J. Salonen, D.Y. Murzin, N. Kumar, T. Laaksonen, L. Peltonen, J. Hirvonen, Drug delivery formulations of ordered and nonordered mesoporous silica: comparison of three drug loading methods, J. Pharmacol. Sci. 100 (2011) 3294–3306, https://doi.org/10.1002/jps.22577.
[45] Y. Zhang, Z. Zhi, T. Jiang, J. Zhang, Z. Wang, S. Wang, Spherical mesoporous silica nanoparticles for loading and release of the poorly water-soluble drug telmisartan, J. Contr. Release 145 (2010) 257–263, https://doi.org/10.1016/j.jconrel.2010.04.029.
[46] M. Otsuka, K. Tokumitsu, Y. Matsuda, Solid dosage form preparations from oily medicines and their drug release. Effect of degree of surface-modification of silica gel on the drug release from phytonadione-loaded silica gels, J. Contr. Release 67 (2000) 369–384, https://doi.org/10.1016/s0168-3659(00)00229-7.
[47] W.D. Callister, D.G. Rathwisch, Fundamentals of Materials Science and Engineering: an Integrated Approach, fifth ed., Wiley, London, UK, 2000, 471660817.
[48] R. Dagil, C. O'shea, A. Nykjær, A.M. Bonvin, B.B. Kragelund, Gentamicin binds to the megalin receptor as a competitive inhibitor using the common ligand binding motif of complement type repeats, J. Biol. Chem. 288 (2013) 4424–4435, https://doi.org/10.1074/jbc.M112.434159.
[49] M.K. Phillips-Jones, R. Lithgo, V. Dinu, R.B. Gillis, J.E. Harding, G.G. Adams, S. E. Harding, Full hydrodynamic reversibility of the weak dimerization of vancomycin and elucidation of its interaction with VanS monomers at clinical concentration, Sci. Rep. 7 (2017) 12697, https://doi.org/10.1038/s41598-017-12620-z.
[50] S. Yoshioka, V.J. Stella, Stability of Drugs and Dosage Forms, Springer Science & Business Media, 2000, https://doi.org/10.1007/b114443.
[51] EFSA Panel on Contaminants in the Food Chain, Scientific opinion on nitrofurans and their metabolites in food, EFSA J 13 (2015) 4140, https://doi.org/10.2903/j.efsa.2015.4140.
[52] M. Biošić, I. Škorić, J. Beganović, S. Babić, Nitrofurantoin hydrolytic degradation in the environment, Chemosphere 186 (2017) 660–668, https://doi.org/10.1016/j.chemosphere.2017.08.011.
[53] J. Comer, S. Judge, D. Matthews, L. Towes, B. Falcone, J. Goodman, J. Dearden, The intrinsic aqueous solubility of indomethacin, ADMET & DMPK 2 (2014) 18–32, https://doi.org/10.5599/admet.2.1.33.
[54] F. Temussi, F. Cermola, M. Della Greca, M.R. Iesce, M. Passananti, L. Previtera, A. Zarrelli, Determination of photostability and photodegradation products of indomethacin in aqueous media, J. Pharmaceut. Biomed. Anal. 56 (2011) 678–683, https://doi.org/10.1016/j.jpba.2011.07.005.
[55] S.C. Chow, J. Shao, Estimating drug shelf-life with random batches, Biometrics 47 (1991) 1071–1079, https://doi.org/10.2307/2532659.